HHS Public Access

Author manuscript

J Chem Inf Model. Author manuscript; available in PMC 2024 March 28.

Published in final edited form as:

J Chem Inf Model. 2023 November 27; 63(22): 7180–7188. doi:10.1021/acs.jcim.3c01269.

Discovery of nirmatrelvir resistance mutations in SARS-CoV-2 3CLpro: A computational-experimental approach

Brandon Havranek[1,2], **Robel Demissie**[3,4], **Hyun Lee**[3,4], **Shuiyun Lan**[5,6], **Huanchun Zhang**[5,6], **Stefan G. Sarafianos**[5,6], **Anoklase Jean-Luc Ayitou**[7], **Shahidul M. Islam**[2,8,*]

[1]Sidney Kimmel Medical College at Thomas Jefferson University, Philadelphia, PA 19107, USA

[2]ComputePharma, LLC., Chicago, IL, USA, 60607

[3]Department of Pharmaceutical Sciences, College of Pharmacy, University of Illinois at Chicago, Chicago, IL 60607, USA

[4]Biophysics Core at Research Resource Center, University of Illinois at Chicago, Chicago, IL 60607, USA

[5]Center for ViroScience and Cure, Laboratory of Biochemical Pharmacology, Department of Pediatrics, Emory University School of Medicine, Atlanta, GA 30322, USA

[6]Children's Healthcare of Atlanta, Atlanta, GA 30322, USA

[7]Department of Chemistry, University of Illinois Chicago, Chicago, Illinois 60607, USA

[8]Department of Chemistry, Delaware State University, Dover, DE, 19901, USA

Abstract

The COVID-19 pandemic has emphasized the urgency for effective antiviral therapies against SARS-CoV-2. Targeting the main protease (3CLpro) of the virus has emerged as a promising approach, and nirmatrelvir (PF-07321332), the active component of Pfizer's oral drug Paxlovid, has demonstrated remarkable clinical efficacy. However, the emergence of resistance mutations poses a challenge to its continued success. In this study, we employed alchemical free energy perturbation (FEP) alanine scanning to identify nirmatrelvir-resistant mutations within the SARS-CoV-2 3CLpro. FEP identified several mutations, which were validated through in vitro IC_{50} experiments and found to result in 8 and 72-fold increases in nirmatrelvir IC_{50} values. Additionally, we constructed SARS-CoV-2 omicron replicons containing these mutations, and one of the mutants (S144A/E166A) displayed a 20-fold increase in EC_{50}, confirming the role of FEP in identifying drug-resistance mutations. Our findings suggest that FEP can be a valuable tool in proactively monitoring the emergence of resistant strains and guiding the design of future inhibitors with reduced susceptibility to drug resistance. As nirmatrelvir is currently widely used

*Correspondence: sislam@desu.edu.

Author Contributions

B.H. and S.M.I designed the study and wrote the manuscript with input from all authors. B.H. performed all FEP computational simulations and analyses. R.D. and H.L. expressed and purified proteins, performed enzymatic, IC_{50}, and K_i experiments. S.L., H.Z. and S.G.S. performed the replicon experiments. S.M.I. and A.J.L.A secured funding and supervised the work.

Competing Interests

The authors declare no competing interests.

for treating COVID-19, this research has important implications for surveillance efforts and antiviral development.

Introduction

The disastrous COVID-19 pandemic, caused by the severe acute respiratory syndrome coronavirus 2 (SARS-CoV-2), has highlighted the urgent need for effective antiviral therapies to mitigate the disease's impact and complement vaccination strategies.[1] Targeting the main protease (M^{pro}) of SARS-CoV-2, also known as 3-chymotrypsin-like protease (3CLpro), has emerged as a promising approach developing antiviral treatments.[2–6] The 3CLpro is pivotal for viral replication as it cleaves viral polyproteins pp1a and pp1ab at 11 distinct sites, generating nonstructural proteins essential for the viral life cycle.[7,8] Given that human proteases do not recognize these cleavage sites, 3CLpro serves as an attractive and selective drug target.[9]

Nirmatrelvir (PF-07321332), the active component of Pfizer's oral drug Paxlovid, is a peptidomimetic covalent inhibitor of 3CLpro that was granted Emergency Use Authorization by the FDA in December of 2021. Nirmatrelvir has exhibited remarkable clinical efficacy in reducing the risk of hospitalization or death by 89% when administered during the early stages of infection.[10] Unlike other approved SARS-CoV-2 antivirals, such as remdesivir and molnupiravir, nirmatrelvir offers distinct advantages. Remdesivir, a nucleotide analog targeting the viral RNA-dependent RNA polymerase, has shown limited effectiveness in patients requiring ventilation and high-flow oxygen and also requires parenteral administration, restricting its use to hospital settings.[11] Molnupiravir, a nucleoside analog that induces mutations in the viral RNA genome, offers a 31% reduction in hospitalization or death, falling short of nirmatrelvir's 89% reduction.[12] Nirmatrelvir's superior efficacy and oral administration establish it as a more favorable option for patients at high risk of progressing to severe COVID-19.

Nevertheless, the emergence of resistance mutations in the 3CLpro poses a significant challenge to the continued success of nirmatrelvir as an antiviral treatment. A recent Pfizer report directed for healthcare providers disclosed a nirmatrelvir-resistant mutant, S144A, with remarkedly reduced binding to nirmatrelvir (i.e., >90-fold increase in K_i).[13] Similarly, recent reports have reported the presence of nirmatrelvir resistance mutations in SARS-CoV-2 isolates, either generated *de novo* through *in vitro* passaging[14–18] or found in clinical samples.[19–21] SARS-CoV-2 drug-resistant variants have also been previously reported in patients treated with viral polymerase inhibitor remdesivir.[22,23] The development of antiviral resistance is not a novel phenomenon, as evidenced by treating chronic or persistent viral infections such as HIV, hepatitis B virus (HBV), hepatitis C virus (HCV), herpesviruses, and influenza.[24] In these cases, antiviral administration, particularly as monotherapy, has led to the emergence of viral escape mutations, which can compromise therapeutic effectiveness and contribute to treatment failure.[25,26] Thus, identifying nirmatrelvir resistance mutations and providing a detailed understanding of the mechanisms underlying resistance is crucial to minimize the risk of treatment failure, and can further be used to guide the design of inhibitors with reduced potential of evolving viral resistance.

Herein, we used alchemical free energy perturbation (FEP) alanine scanning to identify nirmatrelvir resistance mutations within the SARS-CoV-2 3CLpro. Potential resistance mutations, identified using FEP, were combined in two mutation combinations in recombinant 3CLpro proteins to verify our computational calculations. In vitro IC_{50} experiments of the 3CLpro mutants revealed 8 and 72-fold increases in IC_{50} values of nirmatrelvir. Furthermore, we constructed SARS-CoV-2 replicons on the omicron BA.1 strain background containing our 3CLpro mutations and found a 20-fold increase in EC_{50}, showcasing that FEP can be used successfully to identify drug resistance mutations within the 3CLpro.

Results and Discussion

Free-energy perturbation (FEP) alanine scanning to identify nirmatrelvir resistance mutations

The implementation of alanine scanning mutagenesis (ASM) as a computational technique for examining protein-protein and protein-ligand interactions has proven to be highly effective in elucidating the structural and energetic properties of hot spots and identifying drug-resistance mutations.[27–29] Combining alchemical free energy perturbation with all-atom molecular dynamics simulations (FEP/MD) is arguably the most precise computational strategy for determining the impact of mutations on molecular complexes.[30–34] Using alchemical FEP/MD, we performed alanine scanning on a subset of 3CLpro residues within 4 Å of the nirmatrelvir binding site (PDB ID: 7VH8) (Figure 1a and Figure 1c).[35] We refrained from conducting alchemical FEP/MD alanine scanning on residues H41, C145, and H163 within the 3CLpro, as these residues have been identified as essential for 3CLpro's enzymatic activity.[21,36,37] H41 forms the catalytic dyad with C145. Consequently, it is improbable that these residues would naturally mutate to provide resistance against nirmatrelvir. Furthermore, we deliberately refrained from mutating P168 due to challenges in achieving optimal convergence and parameterization owing to the intricacies of the proline side chain and G143 to conserve computational resources, considering that glycine already possesses a minimal amino acid sidechain (Figure 1a). In total, ASM via FEP was performed for 16 residues in the 3CLpro (Figure 1b and Table 1).

We hypothesized that by introducing alanine mutations that diminish the binding affinity of nirmatrelvir to the 3CLpro, we would consequently reduce the effectiveness of nirmatrelvir. Additionally, we employed FEP/MD alanine scanning as a valuable technique to pinpoint "hot spot" residues within the 3CLpro that are crucial for nirmatrelvir's binding. This approach could reveal targets for future nirmatrelvir-resistant mutations, beyond the scope of alanine mutations alone. In line with best practices[38], all FEP calculations were run bidirectionally (i.e., forward and backward transformations) and free-energy changes were calculated using the maximum-likelihood BAR estimator.[39]

Numerous residues in the 3CLpro enzyme, including M49, N142, L167, and H172, exhibited considerable tolerance to alanine substitutions in our FEP calculations, as demonstrated by a $\Delta\Delta G_{FEP}$ value of ± 0.25 kcal/mol (Table 1). In a recent study, Flynn et al. conducted an exhaustive mutational scan of the 3CLpro to identify mutations that are compatible with the 3CLpro's functionality.[40] Their findings were in line with our results,

revealing that residues M49 and N142 are indeed highly tolerant to mutations, thereby suggesting their potential to facilitate the development of resistance. Although M49A and N142A mutations displayed minimal impact on the binding affinity to nirmatrelvir, it is plausible that non-alanine substitutions could have a more significant influence on binding. Consequently, nirmatrelvir may acquire resistance through alternative mechanisms, aside from the loss of binding affinity via these specific residues. Additional investigations have substantiated the findings of Flynn et al.[40], demonstrating that residues M49 and N142 can accommodate various mutations without substantially compromising enzymatic activity or nirmatrelvir sensitivity.[19,41] These observations suggest that although these residues exhibit high tolerance to mutations, alterations at these sites do not markedly alter the binding affinity of nirmatrelvir to the 3CLpro, as evidenced by our free energy perturbation (FEP) calculations (Table 1 and Figure 1b). Consequently, the sensitivity to nirmatrelvir is preserved despite the presence of mutations at these positions.

In FEP calculations, mutations Y54A, S144A, and E166A significantly reduced nirmatrelvir binding (i.e., $\Delta\Delta G_{FEP} > 1$kcal/mol) (Table 1). Interestingly, S144A and E166A have been found in numerous studies to significantly decrease nirmatrelvir efficacy, including *in vitro* passaging studies[14,16,17] and studies investigating natural 3CLpro polymorphisms.[41] In the course of nirmatrelvir's clinical development, researchers utilized the murine CoV MHV-A59 to examine resistance. They discovered that the S144A mutation resulted in a more than 90-fold decrease in nirmatrelvir's binding efficacy (Ki) to recombinant 3CLpro *in vitro*.[13] Furthermore, the Y54A mutation was associated with a 24-fold increase in the Ki of nirmatrelvir to recombinant 3CLpro.[13] Although the clinical implications of these substitutions remain uncertain, our findings clearly demonstrate that FEP can identify nirmatrelvir-resistance mutations consistent with experimental biochemical assays. Additionally, Heilmann and colleagues[15] detected a similar Y54C mutation in an *in vitro* passaging study using a vesicular stomatitis virus (VSV)-based system, which exhibited some resistance to nirmatrelvir.

Taken together, these results effectively demonstrate the ability of FEP in accurately identifying residues essential for nirmatrelvir binding, as well as those that play a role in fostering resistance against nirmatrelvir, in accordance with existing experimental studies. In particular, S144 and E166 seem to be hot spots for drug resistance of nirmatrelvir.[14,41,42] Overall, these findings suggest that FEP can be useful to not only identify residues that may subsequently mutate to confer resistance to nirmatrelvir via loss in binding affinity, but also in identifying residues within proteins that may be highly tolerant to mutations as evidenced by M49 and N142.

IC_{50} of nirmatrelvir against wild-type and mutant SARS-CoV-2 3CLpro

Next, we cloned and purified two double mutants, Y54A/S144A and S144A/E166A, along with wild-type SARS-CoV-2 3CLpro. Residues Y54 and S144 are located near the catalytic dyad, and all three mutation sites are involved in nirmatrelvir binding (Figure 2a). We designed these two double mutant 3CLpro based upon our FEP calculations (Table 1). Mutations Y54A, S144A, and E166A ($\Delta\Delta G > 1$kcal/mol in FEP) were combined in two mutation combinations to model natural resistance to nirmatrelvir. Recombinant 3CLpro

proteins with Y54A/S144A and S144A/E166A mutations had their enzymatic activities tested by a FRET assay using the peptide substrate 5-FAM-TSATLQ SGFRK(QXL520)-NH2 (Figure 2b). Compared with the wild-type 3CLpro, both double mutants displayed significantly reduced enzymatic activities. At equivalent 125 nM concentration of enzyme, 3CLpro mutants Y54A/S144A and S144A/E166A had 1 and 2% of the activity of the wild-type protein, respectively (Figure 2b). The loss in enzymatic activity may be due to loss of substrate binding and/or potential loss of protein stability and reduced dimerization of the 3CLpro.

All these mutations have been previously selected for *in vitro* passaging studies or identified as natural 3CLpro variants; however, the effect of these mutations combinations on nirmatrelvir resistance have not yet been tested.[13–15,17] Therefore, we hypothesized that these mutations might be plausible to combine to confer resistance to nirmatrelvir. Inhibitory activities (IC_{50}) of nirmatrelvir against wild-type and two double mutants were compared (Figure 3a). The 3CLpro mutants showed significantly decreased activity, so we used a 3.2 times higher 3CLpro enzyme concentration for the mutants. Our assay confirmed that nirmatrelvir is a nanomolar inhibitor of wild-type 3CLpro, with an IC_{50} value of 0.050 ± 0.005 μM (Figure 3a), in agreement with previous reported IC_{50} values of 0.022 and 0.023 μM.[17,19] Consistent with our FEP calculations, the IC_{50} value of nirmatrelvir against the 3CLpro mutant Y54A/S144A was 0.400 ± 0.101 μM, which corresponds to an ~8-fold increase compared to the wild-type 3CLpro (Figure 3a). In addition, the IC_{50} value of nirmatrelvir against the 3CLpro mutant S144A/E166A was 3.60 ± 0.64 μM, which is ~72-fold higher than the wild-type 3CLpro protein (Figure 3a). Therefore, we show that free energy perturbation calculations can reasonably predict nirmatrelvir resistance mutations that substantially decrease IC_{50} efficacy as evidenced by our enzymatic FRET assay. The Ki value of nirmatrelvir against wild-type 3CLpro was determined at 0.012 μM (Figure 3b).

Although the 3CLpro mutants Y54A/S144A and S144A/E166A displayed 8-fold and 72-fold IC_{50} resistance to nirmatrelvir, they also have severely reduced fitness overall, which may compromise their ability to combine and confer resistance in nature. Mutations L50F and T21I have previously been reported to restore replicative fitness.[14,18] Therefore, the addition of these mutations may help to restore fitness of the Y54A/S144A and S144A/E166A 3CLpro mutants.

SARS-CoV-2 omicron BA.1 replicon susceptibility to nirmatrelvir

Lastly, we constructed SARS-CoV-2 replicons on the omicron BA.1 strain background containing 3CLpro mutations Y54A/S144A and S144A/E166A (Table 2).

Compared to wild-type the omicron BA.1 virus and replicon contain 13 mutations at various nonstructural protein genes (nsp), including a single mutation, P132H, in the nsp5 (3CLpro) gene. SARS-CoV-2 replicons allow for the evaluation of nirmatrelvir resistance without conducting heavily regulated gain-of-function experiments using infectious virus. The replicon systems provide a biologically safe alternative to infectious SARS-CoV-2 that recapitulate a large part of the viral replication cycle.[18,43] Consistent with previous studies[44,45], nirmatrelvir remained effective at neutralizing omicron BA.1 with an EC_{50} of 0.11 ± 0.02 μM (Table 2). In comparison, our 3CLpro mutant discovered using FEP, S144A/

E166A, constructed in the omicron BA.1 replicon had an EC_{50} of 2.22 ± 0.41 μM (Table 2), indicating ~20-fold resistance to nirmatrelvir in agreement with our IC_{50} experiments (Fig. 3a).

We also attempted to characterize the Y54A/S144A 3CLpro mutant in omicron BA.1 replicon. However, the SARS-CoV-2 BA.1 replicon with the Y54A/S144A mutations in 3CLpro was not viable due to a significant loss in replicon fitness, which is consistent with our enzymatic activity FRET assay (Figure 2b). Similar to our discussion on the reduced enzymatic activity of our mutants (see above), the addition of mutations L50F and T21I in the 3CLpro have previously shown to restore the replicative fitness of SARS-CoV-2.[14,18] As the potential of drug resistance mutations also depends on the fitness of the virus, additional compensatory mutations that increase virus fitness would likely need to accompany Y54A/S144A and S144A/E166A mutations in the SARS-CoV-2 3CLpro.

Conclusion

As the utilization of nirmatrelvir continues, it brings forth the potential for mutations to arise in the 3CLpro enzyme, granting resistance to nirmatrelvir—a phenomenon that has been observed in relation to other viruses.[46] Moreover, recent developments have shown that antibody therapeutics and other treatment methods against SARS-CoV-2 have proven ineffective against new omicron subvariants.[47] Considering that nirmatrelvir is currently the most widely used antiviral drug for treating COVID-19, it is important to proactively identify and characterize nirmatrelvir-resistant strains before they become prevalent in the population. To address this concern, we employed alchemical free energy perturbation (FEP) techniques to identify mutations within the 3CLpro that confer resistance to nirmatrelvir. The mutations identified through FEP were then validated using an IC_{50} FRET assay, which demonstrated significant decreases—by 8-fold and 72-fold, respectively—in nirmatrelvir's inhibitory capacity against the Y54A/S144A and S144A/E166A 3CLpro mutants. Furthermore, we characterized the S144A/E166A 3CLpro mutant within a SARS-CoV-2 omicron BA.1 replicon. Our findings revealed that this mutant exhibited a 20-fold resistance to nirmatrelvir. Collectively, our IC_{50} and EC_{50} experiments successfully showcase the efficacy of FEP in identifying 3CLpro mutations that confer resistance to nirmatrelvir. We show that combining FEP with biochemical experiments provides a valuable tool for actively monitoring the emergence of 3CLpro mutants in SARS-CoV-2. This research holds significant implications for surveillance efforts and can guide the strategic design of future 3CLpro inhibitors with reduced susceptibility to drug resistance.

Methods

Alchemical free-energy perturbation (FEP) alanine scanning

All FEP/MD simulations were carried out for both the bound (3CLpro-nirmatrelvir) and the free state (3CLpro) using GPU accelerated NAMD 3.0.[48,49] We used PDB: 7VH8 which contains the X-ray crystal structure of SARS-CoV-2 3CLpro in complex with nirmatrelvir solved at 1.59 Å resolution.[35] A series of *in silico* alanine scanning mutations and necessary input files for FEP calculations were generated for 3CLpro residues within 4 Å of the nirmatrelvir binding site using the alanine scanning plugin of VMD.[50] Before FEP

calculations, the corresponding bound (3CLpro-nirmatrelvir) and the free state (3CLpro) systems underwent 2 ns of equilibration MD simulations. The systems force fields were prepared using the CHARMM-GUI webserver[51] utilizing the CHARMM36m additive force field for proteins[52] and CGenFF[53] for ligands. TIP3P was used to model water.[54] In order to mimic physiological conditions, 0.15 M of NaCl ions were added using the Monte-Carlo ion placing method. Periodic boundary conditions (PBC) were applied to all simulations and the particle-mesh-Ewald (PME) method[55] was used to treat all long-range interactions between atoms and the cut-off for non-bonded atom interactions was set to 12 Å. The temperature was kept constant at 300 K using the Langevin thermostat[56,57] and pressure was kept constant at 1.0315 bar using the Nose-Hoover Langevin piston method.[58] All bonds involving hydrogen were constrained using the SHAKE algorithm[59] and water was restrained using the SETTLE algorithm.[60] The integration time step of dynamics was set to 2-fs.

After equilibrating the structures in the bound and free states, we performed FEP calculations.[31,61] For each system, a decoupling (forward) and coupling (backward) transformation were performed in line with best practices.[38] In the alchemical perturbation method, many intermediate stages (denoted by λ) whose Hamiltonian $H(\lambda) = \lambda H_f + (1 - \lambda)H_i$ are inserted between the initial and final states. For each system, λ varies from 0 to 1.0 (for forward transformations) and 1.0 to 0 (for backward transformations) using 20 perturbation windows. Each window consisted of a 200 ps equilibration trajectory followed by a 1 ns production run. Each system (i.e., bound and the free state) underwent 20 ns of production simulation for a total of 40 ns FEP simulations for each alanine mutation calculation. The aggregate simulation time for 16 FEP calculations was 640 ns. The ParseFEP toolkit[62] implemented in VMD[63] was used to test the convergence of the FEP simulations and to compute the free-energy changes and their statistical uncertainties using the maximum-likelihood Bennet Acceptance Ratio (BAR) estimator.[39] The level of stratification between the backward and forward transformations all exhibited a hysteresis smaller than 0.18 kcal/mol, indicating the FEP calculations are well converged.

Construction of the SARS-CoV-2 subgenomic replicon (SARS-2R)

SARS-CoV-2 replicon (SARS-2R) NSP5 mutants (Y54A/S144A, S144A/E166A) of Omicron BA.1 were constructed in the wild-type background as previously described.[43] Briefly, NSP5 mutations were introduced into PCR fragments with primers [SEM957 GTTAATAATTGGTTGAAGCAGTTAATTAAAGTTACACTTGTGTTCCTTTTTG (PacI), SEM624 CGTTCACCTAAGTTGGCGTATACGCG (MluI), SEM1079 GTAAATCTTCAgcATTAGGGTTAAGCATGTCTTCAGAGG (Y54A as), SEM1080 GCTTAACCCTAATgcTGAAGATTTACTCATTCGTAAGTCTAATC (Y54A s), SEM1081 CCAACACTACCACATGcACCATTAAGGAATGAACCCTTAATAG (S144A as), SEM1082 CCTTAATGGTgCATGTGGTAGTGTTGGTTTTAACATAG (S144A s), SEM1083 CCAGTTGGTAATgCCATATGGTGCATGTAACAAAAAGAG (E166A as), SEM1084 CATGCACCATATGGcATTACCAACTGGAGTTCATGCTGGC (E166A s)] and Q5 Hi-Fidelity 2X master mix (NEB, Cat# M0492S). Gel purified PCR fragments were assembled into wild type Omicron BA.1 replicon vector between restriction sites PacI and MluI with NEBuilder® HiFi DNA Assembly Master Mix (Cat# E2621L). All sequences

were validated by long-read sequencing (Plasmidsaurus, Eugene, OR, USA). Sequencing results were analyzed with Lasergene/DNASTAR software (Madison, WI, USA).

Expression and purification of SARS-CoV-2 3CL^{pro}

The full-length SARS-CoV-2 3CL^{pro} gene was codon-optimized, synthesized, and cloned into pGEX6p-1 expression vector with HRV cleavable his6-tag at the C-terminus. The overall overexpression and purification procedures were done similarly as described.[64] In short, 2 L of BL21(DE3) cells containing plasmid with SARS-CoV-2 3CL^{pro} gene were grown to an OD_{600} of 0.7 at 37 °C in LB medium followed by 0.5 mM IPTG induction for 15 hours at 25 °C. Harvested cells were lysed by sonication and purified by a two-step (1 mL HisTrap affinity-16/60 Superdex 75 SEC) purification protocol using AKTA Pure FPLC. The his6-tag was cleaved by HRV protease, producing native 3CL^{pro} proteins. Two double mutants were generated using the wild-type as a template, and overexpression and purification were done similar to the wild-type.

IC_{50} value determination by dose response curve

Nirmatrelvir was initially prepared as 10 mM stocks in 100% DMSO and prepared as 50X of a series of increasing concentrations (0.0051 to 100 μM final concentration at 3-fold serial dilution) in 100% DMSO in a 384-well PCR plate. 50X of nirmatrelvir solutions were further diluted to 3X final concentrations with an assay buffer (50 mM Tris, pH 7.3, 2 mM DTT, and 1 mM EDTA). 3X of the 3CLpro enzyme (125 nM final concentration) was prepared in the same assay buffer. 7 μL each of 375 nM (3X) enzyme solution was distributed into a black low volume 384-well plate wells, and 7 μL of varying concentration of 3X nirmatrelvir were added and incubated for 10 minutes at room temperature. A fluorogenic peptide substrate, 5-FAM-TSATLQSGFRK (QXL520)-NH_2, was initially prepared as 5 mM stock in 100% DMSO and diluted to 3X (15 μM) final concentration in assay buffer. The enzyme reaction was initiated by adding 7 μL of the (3X) substrate, and its activity was continuously monitored for 20 minutes by measuring fluorescence intensity at 490 nm/520 nm (excitation/emission) wave lengths with a BMG Labtech Optima microplate reader. The IC_{50} values were calculated by fitting with the 3 parameter Hill equation (1), using Sigmaplot v14.5 where y is percent inhibition, x is inhibitor concentration, n is the slope of the concentration–response curve (Hill slope), and V_{max} is maximal inhibition from two to four independent assays.

$$y = V_{max}\left(\frac{x^n}{IC_{50}^n + x^n}\right) \quad (1)$$

K_i determination

The 3CLpro enzyme was prepared in the same way as IC_{50} determination. 7 μL each of 375 nM (3X) enzyme solution was distributed into a black 384-well plate wells, and 7 μL of varying concentration of 3X nirmatrelvir were added and incubated for 10 minutes. A fluorogenic peptide substrate was prepared at 3X final concentration (1.63 –13.0 μM at

2-fold dilution) in assay buffer. The enzyme reaction was initiated by adding 7 μL of the (3X) substrate, and its activity was continuously monitored for 20 minutes by measuring fluorescence intensity at 490 nm/520 nm (excitation/emission) wave lengths with a BMG Labtech Optima microplate reader. The initial velocity of the proteolytic activity of the 3CLpro was calculated by linear regression for the first 6 min of the linear kinetic progress curves. To calculate Ki value, Dixon plot was used by plotting nirmatrelvir concentration vs 1/rate using SigmaPlot v14.5.

Replicon dose response

HEK293T cells (ATCC #CRL-11268) seeded in a 6-well plate were transfected with 1 μg replicon plasmid (SARS-2R) using jetPRIME transfection reagent (Polyplus transfection, Illkirch-Graffenstaden, France). At 16 h post transfection, cells were trypsinized then seeded into 96-well plates and treated with serial dilutions of nirmatrelvir (Medkoo Biosciences, Cat#555985). NanoLuc luciferase assays were performed 48 h post treatment (Nano-Glo® Luciferase Assay System, Promega Cat# N1150). Dose response curves were calculated with Prism software (Graphpad, San Diego, CA, USA).

Acknowledgments

This work is supported by the COVID-19 High Performance Computing (HPC) Consortium project and used the Extreme Science and Engineering Discovery Environment (XSEDE), which is supported by National Science Foundation grant number ACI-1548562. This work used the SDSC Expanse supercomputers through allocation CHE210078 to S.M.I. This research has been funded by COBRE (P20GM145765), RCMI (U54MD015959), DE-INBRE (P20GM103446) funded by NIH/NIGMS, PREM (2122158) funded by NSF Division Of Materials Research (DMR) and University of Illinois at Chicago Center for Clinical and Translational Science (CCTS) award (UL1TR002003). NIH funding to S.G.S. is also acknowledged. We would also like to thank Flo Szczepaniak and Dr. Benoit Roux for helpful discussions on the AlaScan plugin.

References

(1). Matrajt L; Brown ER; Cohen MS; Dimitrov D; Janes H. Could Widespread Use of Antiviral Treatment Curb the COVID-19 Pandemic? A Modeling Study. BMC Infect. Dis 2022, 22, 683. 10.1186/s12879-022-07639-1. [PubMed: 35945513]

(2). Quan B-X; Shuai H; Xia A-J; Hou Y; Zeng R; Liu X-L; Lin G-F; Qiao J-X; Li W-P; Wang F-L; Wang K; Zhou R-J; Yuen TT-T; Chen M-X; Yoon C; Wu M; Zhang S-Y; Huang C; Wang Y-F; Yang W; Tian C; Li W-M; Wei Y-Q; Yuen K-Y; Chan JF-W; Lei J; Chu H; Yang S. An Orally Available Mpro Inhibitor Is Effective against Wild-Type SARS-CoV-2 and Variants Including Omicron. Nat. Microbiol 2022, 7, 716–725. 10.1038/s41564-022-01119-7. [PubMed: 35477751]

(3). Qiao J; Li Y-S; Zeng R; Liu F-L; Luo R-H; Huang C; Wang Y-F; Zhang J; Quan B; Shen C; Mao X; Liu X; Sun W; Yang W; Ni X; Wang K; Xu L; Duan Z-L; Zou Q-C; Zhang H-L; Qu W; Long Y-H-P; Li M-H; Yang R-C; Liu X; You J; Zhou Y; Yao R; Li W-P; Liu J-M; Chen P; Liu Y; Lin G-F; Yang X; Zou J; Li L; Hu Y; Lu G-W; Li W-M; Wei Y-Q; Zheng Y-T; Lei J; Yang S. SARS-CoV-2 M pro Inhibitors with Antiviral Activity in a Transgenic Mouse Model. Science. 2021, 371, 1374–1378. 10.1126/science.abf1611. [PubMed: 33602867]

(4). Owen DR; Allerton CMN; Anderson AS; Aschenbrenner L; Avery M; Berritt S; Boras B; Cardin RD; Carlo A; Coffman KJ; Dantonio A; Di L; Eng H; Ferre R; Gajiwala KS; Gibson SA; Greasley SE; Hurst BL; Kadar EP; Kalgutkar AS; Lee JC; Lee J; Liu W; Mason SW; Noell S; Novak JJ; Obach RS; Ogilvie K; Patel NC; Pettersson M; Rai DK; Reese MR; Sammons MF; Sathish JG; Singh RSP; Steppan CM; Stewart AE; Tuttle JB; Updyke L; Verhoest PR; Wei L; Yang Q; Zhu Y. An Oral SARS-CoV-2 M pro Inhibitor Clinical Candidate for the Treatment of COVID-19. Science. 2021, 374, 1586–1593. 10.1126/science.abl4784. [PubMed: 34726479]

(5). Zhang C-H; Stone EA; Deshmukh M; Ippolito JA; Ghahremanpour MM; Tirado-Rives J; Spasov KA; Zhang S; Takeo Y; Kudalkar SN; Liang Z; Isaacs F; Lindenbach B; Miller SJ; Anderson KS; Jorgensen WL Potent Noncovalent Inhibitors of the Main Protease of SARS-CoV-2 from Molecular Sculpting of the Drug Perampanel Guided by Free Energy Perturbation Calculations. ACS Cent. Sci 2021, 7, 467–475. 10.1021/acscentsci.1c00039. [PubMed: 33786375]

(6). Havranek B; Islam SM An in Silico Approach for Identification of Novel Inhibitors as Potential Therapeutics Targeting COVID-19 Main Protease. J. Biomol. Struct. Dyn 2020, 1–12. 10.1080/07391102.2020.1776158.

(7). Thiel V; Ivanov KA; Putics Á; Hertzig T; Schelle B; Bayer S; Weißbrich B; Snijder EJ; Rabenau H; Doerr HW; Gorbalenya AE; Ziebuhr J. Mechanisms and Enzymes Involved in SARS Coronavirus Genome Expression. J. Gen. Virol 2003, 84, 2305–2315. 10.1099/vir.0.19424-0. [PubMed: 12917450]

(8). Ziebuhr J; Heusipp G; Siddell SG Biosynthesis, Purification, and Characterization of the Human Coronavirus 229E 3C-like Proteinase. J. Virol 1997, 71, 3992–3997. 10.1128/jvi.71.5.3992-3997.1997. [PubMed: 9094676]

(9). Dai W; Zhang B; Jiang X-M; Su H; Li J; Zhao Y; Xie X; Jin Z; Peng J; Liu F; Li C; Li Y; Bai F; Wang H; Cheng X; Cen X; Hu S; Yang X; Wang J; Liu X; Xiao G; Jiang H; Rao Z; Zhang L-K; Xu Y; Yang H; Liu H. Structure-Based Design of Antiviral Drug Candidates Targeting the SARS-CoV-2 Main Protease. Science. 2020, 368, 1331–1335. 10.1126/science.abb4489. [PubMed: 32321856]

(10). Duveau DY; Thomas CJ The Remarkable Selectivity of Nirmatrelvir. ACS Pharmacol. Transl. Sci 2022, 5, 445–447. 10.1021/acsptsci.2c00065. [PubMed: 35702394]

(11). Gottlieb RL; Vaca CE; Paredes R; Mera J; Webb BJ; Perez G; Oguchi G; Ryan P; Nielsen BU; Brown M; Hidalgo A; Sachdeva Y; Mittal S; Osiyemi O; Skarbinski J; Juneja K; Hyland RH; Osinusi A; Chen S; Camus G; Abdelghany M; Davies S; Behenna-Renton N; Duff F; Marty FM; Katz MJ; Ginde AA; Brown SM; Schiffer JT; Hill JA Early Remdesivir to Prevent Progression to Severe Covid-19 in Outpatients. N. Engl. J. Med 2022, 386, 305–315. 10.1056/NEJMoa2116846. [PubMed: 34937145]

(12). Focosi D. Molnupiravir: From Hope to Epic Fail? Viruses 2022, 14, 2560. 10.3390/v14112560. [PubMed: 36423169]

(13). FDA. FACT SHEET FOR HEALTHCARE PROVIDERS: EMERGENCY USE AUTHORIZATION FOR PAXLOVID; 2021.

(14). Iketani S; Mohri H; Culbertson B; Hong SJ; Duan Y; Luck MI; Annavajhala MK; Guo Y; Sheng Z; Uhlemann A-C; Goff SP; Sabo Y; Yang H; Chavez A; Ho DD Multiple Pathways for SARS-CoV-2 Resistance to Nirmatrelvir. Nature 2023, 613, 558–564. 10.1038/s41586-022-05514-2. [PubMed: 36351451]

(15). Heilmann E; Costacurta F; Moghadasi SA; Ye C; Pavan M; Bassani D; Volland A; Ascher C; Weiss AKH; Bante D; Harris RS; Moro S; Rupp B; Martinez-Sobrido L; von Laer D. SARS-CoV-2 3CL pro Mutations Selected in a VSV-Based System Confer Resistance to Nirmatrelvir, Ensitrelvir, and GC376. Sci. Transl. Med 2023, 15. 10.1126/scitranslmed.abq7360.

(16). Zhou Y; Gammeltoft KA; Ryberg LA; Pham LV; Tjørnelund HD; Binderup A; Duarte Hernandez CR; Fernandez-Antunez C; Offersgaard A; Fahnøe U; Peters GHJ; Ramirez S; Bukh J; Gottwein JM Nirmatrelvir-Resistant SARS-CoV-2 Variants with High Fitness in an Infectious Cell Culture System. Sci. Adv 2022, 8. 10.1126/sciadv.add7197.

(17). Dirk J; Cheng L; Kim D; Antitsa S; Sandro BK; , S S; Chloe DV; Bert V; Piet M; Bettina T; Nadine E; Volker T; Steven DJ; Laura V; Dorothée B; Andreas JM; , B L; Leonid B; A SJ; Pierre R; Patrick C; Arnaud M; Johan N; Jerome D; Koen V. The Substitutions L50F, E166A, and L167F in SARS-CoV-2 3CLpro Are Selected by a Protease Inhibitor In Vitro and Confer Resistance To Nirmatrelvir. MBio 2023, 14, e02815–22. 10.1128/mbio.02815-22.

(18). Lan S; Neilsen G; Slack RL; Cantara WA; Castaner AE; Lorson ZC; Lulkin N; Zhang H; Lee J; Cilento ME; Tedbury PR; Sarafianos SG Nirmatrelvir Resistance in SARS-CoV-2 Omicron_BA.1 and WA1 Replicons and Escape Strategies. bioRxiv 2023, 2022.12.31.522389. 10.1101/2022.12.31.522389.

(19). Noske GD; de Souza Silva E; de Godoy MO; Dolci I; Fernandes RS; Guido RVC; Sjö P; Oliva G; Godoy AS Structural Basis of Nirmatrelvir and Ensitrelvir Activity against Naturally Occurring

Polymorphisms of the SARS-CoV-2 Main Protease. J. Biol. Chem 2023, 299, 103004. 10.1016/j.jbc.2023.103004.

(20). Moghadasi SA; Heilmann E; Khalil AM; Nnabuife C; Kearns FL; Ye C; Moraes SN; Costacurta F; Esler MA; Aihara H; von Laer D; Martinez-Sobrido L; Palzkill T; Amaro RE; Harris RS Transmissible SARS-CoV-2 Variants with Resistance to Clinical Protease Inhibitors. Sci. Adv 2023, 9. 10.1126/sciadv.ade8778.

(21). Hu Y; Lewandowski EM; Tan H; Zhang X; Morgan RT; Zhang X; Jacobs LMC; Butler SG; Gongora MV; Choy J; Deng X; Chen Y; Wang J. Naturally Occurring Mutations of SARS-CoV-2 Main Protease Confer Drug Resistance to Nirmatrelvir. ACS Cent. Sci 2023, 9, 1658–1669. 10.1021/acscentsci.3c00538. [PubMed: 37637734]

(22). Gandhi S; Klein J; Robertson AJ; Peña-Hernández MA; Lin MJ; Roychoudhury P; Lu P; Fournier J; Ferguson D; Mohamed Bakhash SAK; Catherine Muenker M; Srivathsan A; Wunder EA; Kerantzas N; Wang W; Lindenbach B; Pyle A; Wilen CB; Ogbuagu O; Greninger AL; Iwasaki A; Schulz WL; Ko AI De Novo Emergence of a Remdesivir Resistance Mutation during Treatment of Persistent SARS-CoV-2 Infection in an Immunocompromised Patient: A Case Report. Nat. Commun 2022, 13, 1547. 10.1038/s41467-022-29104-y. [PubMed: 35301314]

(23). Hogan JI; Duerr R; Dimartino D; Marier C; Hochman SE; Mehta S; Wang G; Heguy A. Remdesivir Resistance in Transplant Recipients With Persistent Coronavirus Disease 2019. Clin. Infect. Dis 2023, 76, 342–345. 10.1093/cid/ciac769. [PubMed: 36156117]

(24). Richman DD; Nathanson N. Antiviral Therapy. In Viral Pathogenesis; Elsevier, 2016; pp 271–287. 10.1016/B978-0-12-800964-2.00020-3.

(25). Carey I; Harrison PM Monotherapy versus Combination Therapy for the Treatment of Chronic Hepatitis B. Expert Opin. Investig. Drugs 2009, 18, 1655–1666. 10.1517/13543780903241599.

(26). Strasfeld L; Chou S. Antiviral Drug Resistance: Mechanisms and Clinical Implications. Infect. Dis. Clin. North Am 2010, 24, 413–437. 10.1016/j.idc.2010.01.001. [PubMed: 20466277]

(27). Ibarra AA; Bartlett GJ; Hegedüs Z; Dutt S; Hobor F; Horner KA; Hetherington K; Spence K; Nelson A; Edwards TA; Woolfson DN; Sessions RB; Wilson AJ Predicting and Experimentally Validating Hot-Spot Residues at Protein–Protein Interfaces. ACS Chem. Biol 2019, acschembio.9b00560. 10.1021/acschembio.9b00560.

(28). Friedman R. Computational Studies of Protein–Drug Binding Affinity Changes upon Mutations in the Drug Target. WIREs Comput. Mol. Sci 2022, 12. 10.1002/wcms.1563.

(29). Hauser K; Negron C; Albanese SK; Ray S; Steinbrecher T; Abel R; Chodera JD; Wang L. Predicting Resistance of Clinical Abl Mutations to Targeted Kinase Inhibitors Using Alchemical Free-Energy Calculations. Commun. Biol 2018, 1, 70. 10.1038/s42003-018-0075-x. [PubMed: 30159405]

(30). Havranek B; Lindsey GW; Higuchi Y; Itoh Y; Suzuki T; Okamoto T; Hoshino A; Procko E; Islam SM A Computationally Designed ACE2 Decoy Has Broad Efficacy against SARS-CoV-2 Omicron Variants and Related Viruses in Vitro and in Vivo. Commun. Biol 2023, 6, 513. 10.1038/s42003-023-04860-9. [PubMed: 37173421]

(31). Christophe Chipot AP Free Energy Calculations: Theory and Applications in Chemistry and Biology; Chipot C., Pohorille A., Eds.; Springer Series in CHEMICAL PHYSICS; Springer Berlin Heidelberg: Berlin, Heidelberg, 2007; Vol. 86. 10.1007/978-3-540-38448-9.

(32). Nandigrami P; Szczepaniak F; Boughter CT; Dehez F; Chipot C; Roux B. Computational Assessment of Protein–Protein Binding Specificity within a Family of Synaptic Surface Receptors. J. Phys. Chem. B 2022, 126, 7510–7527. 10.1021/acs.jpcb.2c02173. [PubMed: 35787023]

(33). Luan B; Huynh T. In Silico Antibody Mutagenesis for Optimizing Its Binding to Spike Protein of Severe Acute Respiratory Syndrome Coronavirus 2. J. Phys. Chem. Lett 2020, 11, 9781–9787. 10.1021/acs.jpclett.0c02706. [PubMed: 33147968]

(34). Clayton J; de Oliveira VM; Ibrahim MF; Sun X; Mahinthichaichan P; Shen M; Hilgenfeld R; Shen J. Integrative Approach to Dissect the Drug Resistance Mechanism of the H172Y Mutation of SARS-CoV-2 Main Protease. J. Chem. Inf. Model 2023. 10.1021/acs.jcim.3c00344.

(35). Zhao Y; Fang C; Zhang Q; Zhang R; Zhao X; Duan Y; Wang H; Zhu Y; Feng L; Zhao J; Shao M; Yang X; Zhang L; Peng C; Yang K; Ma D; Rao Z; Yang H. Crystal Structure of SARS-CoV-2

Main Protease in Complex with Protease Inhibitor PF-07321332. Protein Cell 2022, 13, 689–693. 10.1007/s13238-02100883-2. [PubMed: 34687004]

(36). Świderek K; Moliner V. Revealing the Molecular Mechanisms of Proteolysis of SARS-CoV-2 M pro by QM/MM Computational Methods. Chem. Sci 2020, 11, 10626–10630. 10.1039/D0SC02823A.

(37). Jin Z; Du X; Xu Y; Deng Y; Liu M; Zhao Y; Zhang B; Li X; Zhang L; Peng C; Duan Y; Yu J; Wang L; Yang K; Liu F; Jiang R; Yang X; You T; Liu X; Yang X; Bai F; Liu H; Liu X; Guddat LW; Xu W; Xiao G; Qin C; Shi Z; Jiang H; Rao Z; Yang H. Structure of Mpro from SARS-CoV-2 and Discovery of Its Inhibitors. Nature 2020, 582, 289–293. 10.1038/s41586-020-2223-y. [PubMed: 32272481]

(38). Pohorille A; Jarzynski C; Chipot C. Good Practices in Free-Energy Calculations. J. Phys. Chem. B 2010, 114, 10235–10253. 10.1021/jp102971x.

(39). Bennett CH Efficient Estimation of Free Energy Differences from Monte Carlo Data. J. Comput. Phys 1976, 22, 245–268. 10.1016/0021-9991(76)90078-4.

(40). Flynn JM; Samant N; Schneider-Nachum G; Barkan DT; Yilmaz NK; Schiffer CA; Moquin SA; Dovala D; Bolon DN Comprehensive Fitness Landscape of SARS-CoV-2 Mpro Reveals Insights into Viral Resistance Mechanisms. Elife 2022, 11. 10.7554/eLife.77433.

(41). Hu Y; Lewandowski EM; Tan H; Zhang X; Morgan RT; Zhang X; Jacobs LMC; Butler SG; Gongora MV; Choy J; Deng X; Chen Y; Wang J. Naturally Occurring Mutations of SARS-CoV-2 Main Protease Confer Drug Resistance to Nirmatrelvir. bioRxiv 2022, 2022.06.28.497978. 10.1101/2022.06.28.497978.

(42). Sasi VM; Ullrich S; Ton J; Fry SE; Johansen-Leete J; Payne RJ; Nitsche C; Jackson CJ Predicting Antiviral Resistance Mutations in SARS-CoV-2 Main Protease with Computational and Experimental Screening. Biochemistry 2022, 61, 2495–2505. 10.1021/acs.biochem.2c00489. [PubMed: 36326185]

(43). Lan S; Tedbury PR; Ong YT; Shah R; Slack RL; Cilento ME; Zhang H; Du H; Lulkin N; Le U; Kirby KA; Melcak I; Cantara WA; Boggs EA; Sarafianos SG Subgenomic SARS-CoV-2 Replicon and Reporter Replicon Cell Lines Enable Ultrahigh Throughput Antiviral Screening and Mechanistic Studies with Antivirals, Viral Mutations or Host Factors That Affect COVID-19 Replication. bioRxiv 2021, 2021.12.29.474471. 10.1101/2021.12.29.474471.

(44). Ohashi H; Hishiki T; Akazawa D; Kim KS; Woo J; Shionoya K; Tsuchimoto K; Iwanami S; Moriyama S; Kinoshita H; Yamada S; Kuroda Y; Yamamoto T; Kishida N; Watanabe S; Hasegawa H; Ebihara H; Suzuki T; Maeda K; Fukushi S; Takahashi Y; Iwami S; Watashi K. Different Efficacies of Neutralizing Antibodies and Antiviral Drugs on SARS-CoV-2 Omicron Subvariants, BA.1 and BA.2. Antiviral Res. 2022, 205, 105372. 10.1016/j.antiviral.2022.105372.

(45). Huang C; Shuai H; Qiao J; Hou Y; Zeng R; Xia A; Xie L; Fang Z; Li Y; Yoon C; Huang Q; Hu B; You J; Quan B; Zhao X; Guo N; Zhang S; Ma R; Zhang J; Wang Y; Yang R; Zhang S; Nan J; Xu H; Wang F; Lei J; Chu H; Yang S. A New Generation Mpro Inhibitor with Potent Activity against SARS-CoV-2 Omicron Variants. Signal Transduct. Target. Ther 2023, 8, 128. 10.1038/s41392023-01392-w. [PubMed: 36928316]

(46). Purohit R; Rajasekaran R; Sudandiradoss C; George Priya Doss C; Ramanathan K; Rao S. Studies on Flexibility and Binding Affinity of Asp25 of HIV-1 Protease Mutants. Int. J. Biol. Macromol 2008, 42, 386–391. 10.1016/j.ijbiomac.2008.01.011. [PubMed: 18367244]

(47). Planas D; Bruel T; Staropoli I; Guivel-Benhassine F; Porrot F; Maes P; Grzelak L; Prot M; Mougari S; Planchais C; Puech J; Saliba M; Sahraoui R; Fémy F; Morel N; Dufloo J; Sanjuán R; Mouquet H; André E; Hocqueloux L; Simon-Loriere E; Veyer D; Prazuck T; Péré H; Schwartz O. Resistance of Omicron Subvariants BA.2.75.2, BA.4.6, and BQ.1.1 to Neutralizing Antibodies. Nat. Commun 2023, 14, 824. 10.1038/s41467-023-36561-6. [PubMed: 36788246]

(48). Chen H; Maia JDC; Radak BK; Hardy DJ; Cai W; Chipot C; Tajkhorshid E. Boosting Free-Energy Perturbation Calculations with GPU-Accelerated NAMD. J. Chem. Inf. Model 2020, 60, 5301–5307. 10.1021/acs.jcim.0c00745. [PubMed: 32805108]

(49). Phillips JC; Braun R; Wang W; Gumbart J; Tajkhorshid E; Villa E; Chipot C; Skeel RD; Kalé L; Schulten K. Scalable Molecular Dynamics with NAMD. J. Comput. Chem 2005, 26, 1781–1802. 10.1002/jcc.20289. [PubMed: 16222654]

(50). Ramadoss V; Dehez F; Chipot C. AlaScan: A Graphical User Interface for Alanine Scanning Free-Energy Calculations. J. Chem. Inf. Model 2016, 56, 1122–1126. 10.1021/acs.jcim.6b00162. [PubMed: 27214306]

(51). Jo S; Kim T; Iyer VG; Im W. CHARMM-GUI: A Web-Based Graphical UserInterface for CHARMM. J. Comput. Chem 2008, 29, 1859–1865. [PubMed: 18351591]

(52). Lee J; Cheng X; Swails JM; Yeom MS; Eastman PK; Lemkul JA; Wei S; Buckner J; Jeong JC; Qi Y; Jo S; Pande VS; Case DA; Brooks CL; MacKerell AD; Klauda JB; Im W. CHARMM-GUI Input Generator for NAMD, GROMACS, AMBER, OpenMM, and CHARMM/OpenMM Simulations Using the CHARMM36 Additive Force Field. J. Chem. Theory Comput 2016, 12, 405–413. 10.1021/acs.jctc.5b00935. [PubMed: 26631602]

(53). Vanommeslaeghe K; Hatcher E; Acharya C; Kundu S; Zhong S; Shim J; Darian E; Guvench O; Lopes P; Vorobyov I; Mackerell AD CHARMM General Force Field: A Force Field for Drug-like Molecules Compatible with the CHARMM All-Atom Additive Biological Force Fields. J. Comput. Chem 2010, 31, 671–690. 10.1002/jcc.21367. [PubMed: 19575467]

(54). Jorgensen WL; Chandrasekhar J; Madura JD; Impey RW; Klein ML Comparison of Simple Potential Functions for Simulating Liquid Water. J. Chem. Phys 1983, 79, 926–935. 10.1063/1.445869.

(55). Essmann U; Perera L; Berkowitz ML; Darden T; Lee H; Pedersen LG A Smooth Particle Mesh Ewald Method. J. Chem. Phys 1995, 103, 8577–8593. 10.1063/1.470117.

(56). Adelman SA Generalized Langevin Equation Approach for Atom/Solid-Surface Scattering: General Formulation for Classical Scattering off Harmonic Solids. J. Chem. Phys 1976, 64, 2375. 10.1063/1.432526.

(57). Wang X; Chen Y; Deng W. Lévy-Walk-like Langevin Dynamics. New J. Phys 2019, 29, 1–20. 10.1088/1367-2630/aaf764.

(58). Martinetz T; Schulten K. Topology Representing Networks. Neural Networks 1994, 7, 507–522. 10.1016/0893-6080(94)90109-0.

(59). Elber R; Ruymgaart AP; Hess B. SHAKE Parallelization. Eur. Phys. J. Spec. Top 2011, 200, 211–223. 10.1140/epjst/e2011-01525-9. [PubMed: 22368766]

(60). Miyamoto S; Kollman PA Settle: An Analytical Version of the SHAKE and RATTLE Algorithm for Rigid Water Models. J. Comput. Chem 1992, 13, 952–962. 10.1002/jcc.540130805.

(61). Zwanzig RW High-Temperature Equation of State by a Perturbation Method. I. Nonpolar Gases. J. Chem. Phys 1954, 22, 1420–1426. 10.1063/1.1740409.

(62). Liu P; Dehez F; Cai W; Chipot C. A Toolkit for the Analysis of Free-Energy Perturbation Calculations. J. Chem. Theory Comput 2012, 8, 2606–2616. 10.1021/ct300242f. [PubMed: 26592106]

(63). Humphrey W; Dalke A; Schulten K. VMD: Visual Molecular Dynamics. J. Mol. Graph 1996, 14, 33–38. 10.1016/0263-7855(96)00018-5. [PubMed: 8744570]

(64). Lee H; Mittal A; Patel K; Gatuz JL; Truong L; Torres J; Mulhearn DC; Johnson ME Identification of Novel Drug Scaffolds for Inhibition of SARS-CoV 3-Chymotrypsin-like Protease Using Virtual and High-Throughput Screenings. Bioorg. Med. Chem 2014, 22, 167–177. 10.1016/j.bmc.2013.11.041. [PubMed: 24332657]

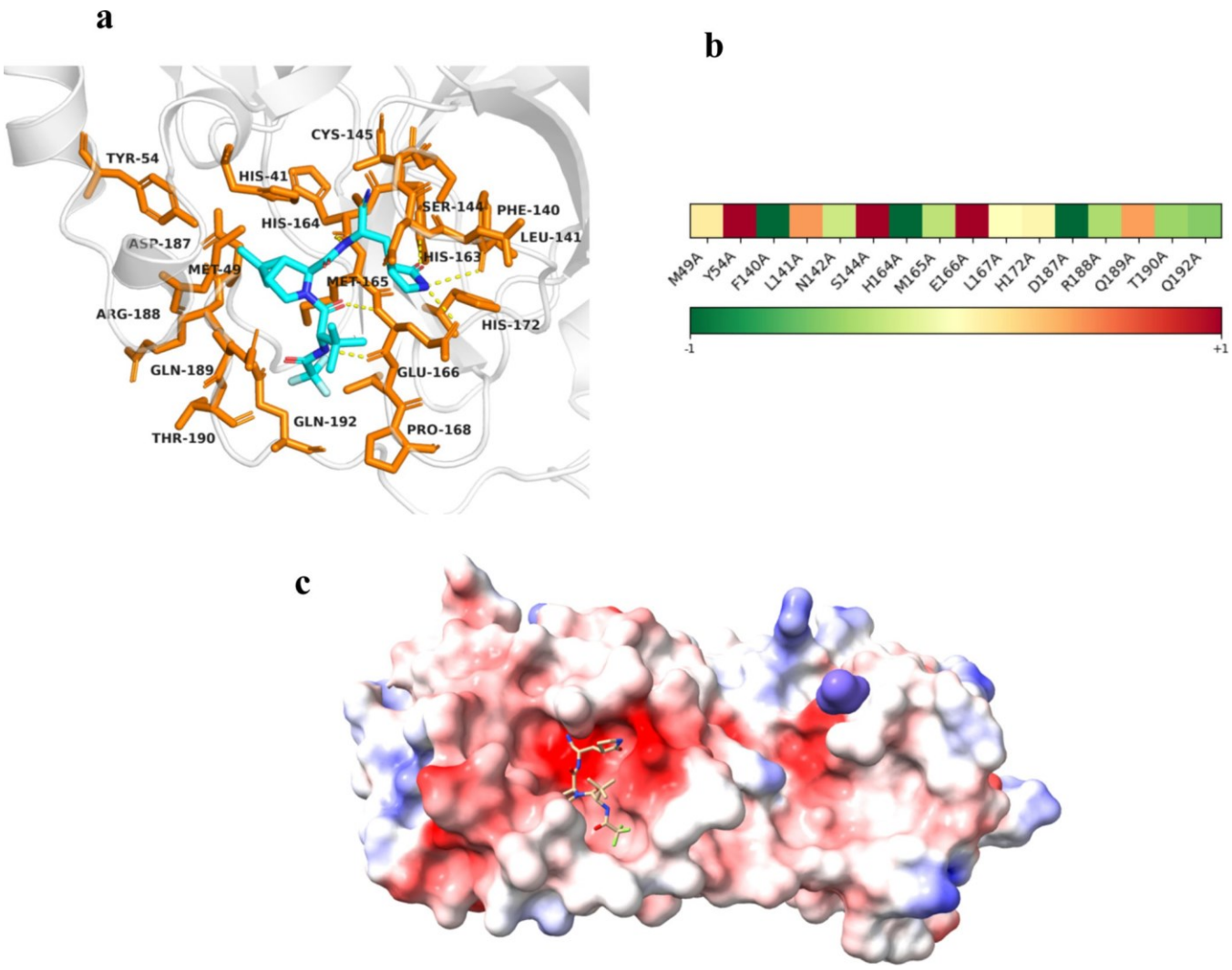

Figure 1. Targeted alanine scanning mutagenesis in 3CLpro using FEP to identify nirmatrelvir resistance mutations.

a. Cartoon representation of nirmatrelvir (blue) in complex with 3CLpro (gray) (PDB:7VH8). Residues in 3CLpro within 4 Å of nirmatrelvir shown as sticks in orange. Yellow lines represent polar contacts between nirmatrelvir and 3CLpro. **b.** Heat map showcasing computed changes in free energy of binding (kcal/mol) for alanine mutations in 3CLpro and binding with nirmatrelvir. All binding values are rescaled from −1 (alanine mutations increase binding with nirmatrelvir shown in green) to +1 (alanine mutations decrease binding with nirmatrelvir shown in red). **c.** Nirmatrelvir in complex with 3CLpro. 3CLpro shown in electrostatics. Red and blue for negative and positive charges, respectively.

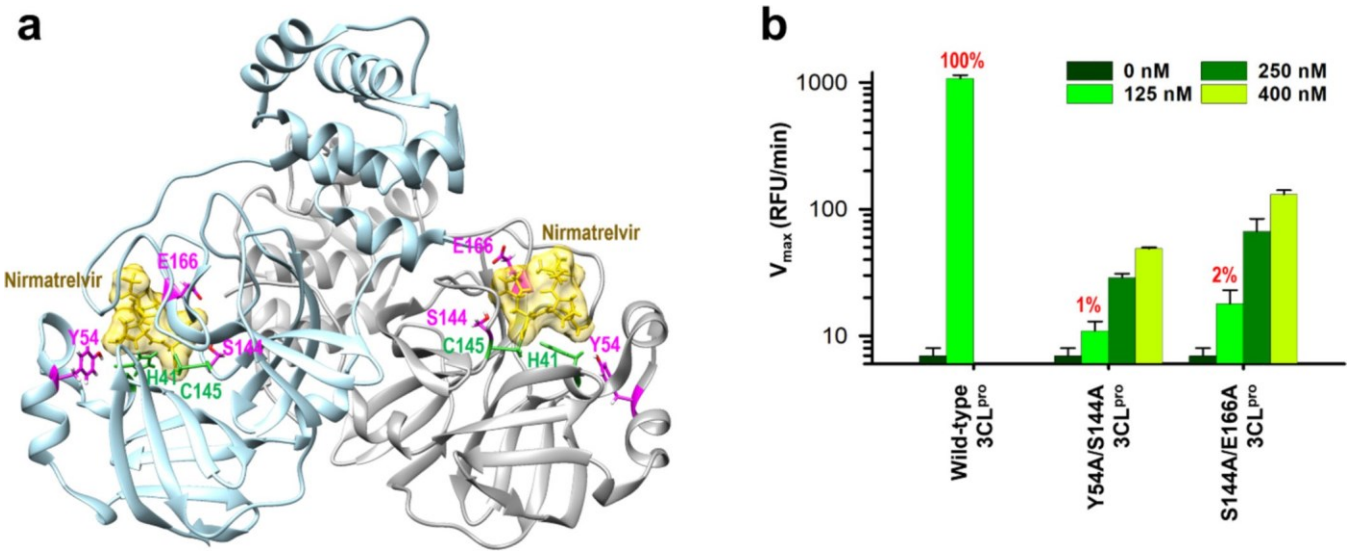

Figure 2. Protease activity comparison of the wild-type and two 3CLpro mutants.

a. Dimer form of SARS-CoV-2 3CLpro structure complexed with nirmatrelvir (PDB code: 8DZ2). Residues of three mutation sites and catalytic dyad are shown in magenta and green, respectively, along with nirmatrelvir in gold color. **b.** 3CLpro mutants Y54A/S144A and S144A/E166A have severely diminished enzymatic activity compared to wild-type. The enzymatic activity of wild-type and mutant 3CLpro were measured and compared in a FRET assay using 125 nM, 250 nM, and 400 nM of 3CLpro enzyme. The FRET assay was conducted in triplicate (n = 3) and the mean with the standard deviation (SD) is shown.

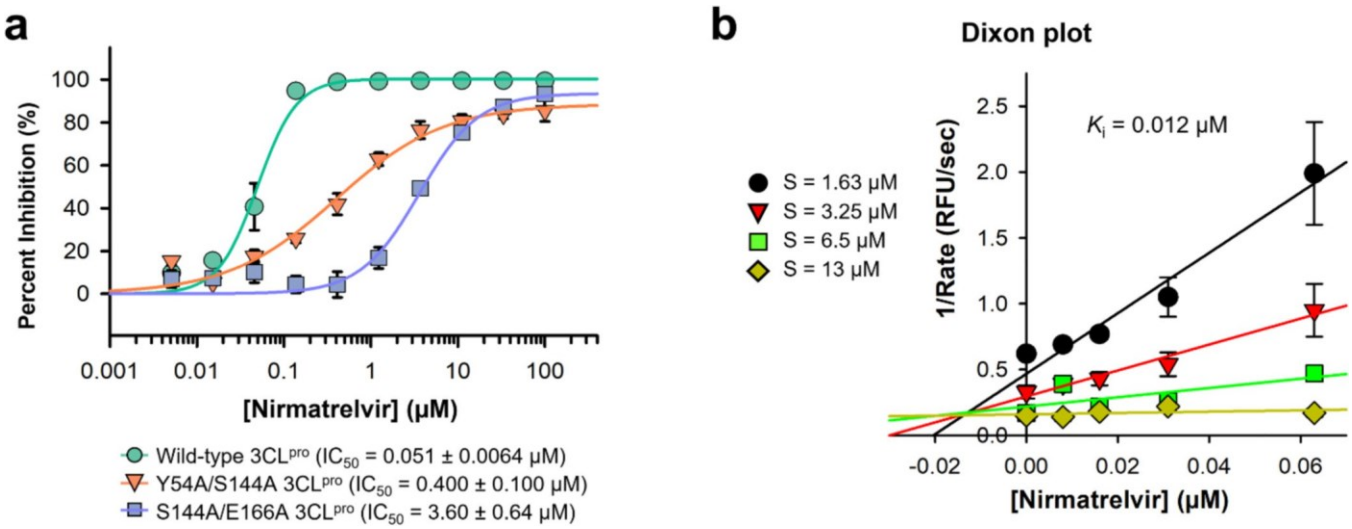

Figure 3. Nirmatrelvir resistance of 3CLpro mutants.

a. IC_{50} values of nirmatrelvir to wild-type and Y54A/S144A and S144A/E166A 3CLpro mutants were determined using a FRET assay. The values represent the mean and standard deviation (SD) from n = 3 replicates. **b**. Kinetics of inhibition of 3CLpro activity by nirmatrelvir. Dixon plot for competitive inhibition is shown.

Table 1.

Alanine scanning mutagenesis with FEP (kcal/mol) identifies nirmatrelvir resistance mutations.[a]

Mutation	3CLpro-nirmatrelvir $\Delta G_{\text{Bound state}}$ [c]	3CLpro $\Delta G_{\text{Free state}}$ [c]	$\Delta\Delta G_{\text{FEP}}$ [b]
M49A	2.35 ± 0.09	2.24 ± 0.10	0.11
Y54A	12.37 ± 0.17	9.41 ± 0.10	2.96
F140A	−9.13 ± 0.15	−7.62 ± 0.04	−1.52
L141A	12.17 ± 0.07	11.71 ± 0.07	0.46
N142A	77.32 ± 0.04	77.57 ± 0.03	−0.25
S144A	−2.85 ± 0.08	−5.77 ± 0.08	2.92
H164A	18.92 ± 0.10	21.10 ± 0.12	−2.18
M165A	2.32 ± 0.09	2.63 ± 0.06	−0.31
E166A	109.68 ± 0.10	108.38 ± 0.12	1.30
L167A	14.81 ± 0.10	14.81 ± 0.11	0.002
H172A	21.16 ± 0.13	21.11 ± 0.16	0.06
D187A	131.50 ± 0.11	133.39 ± 0.18	−1.88
R188A	267.10 ± 0.12	267.47 ± 0.18	−0.36
Q189A	56.59 ± 0.07	56.15 ± 0.07	0.44
T190A	18.08 ± 0.05	18.51 ± 0.04	−0.42
Q192A	56.53 ± 0.06	57.02 ± 0.06	−0.50

[a] When $\Delta\Delta G_{\text{FEP}} > 0$ mutations to alanine are less favorable in the bound state than in the free state.

[b] $\Delta\Delta G_{\text{FEP}}$ is calculated where $\Delta\Delta G_{\text{FEP}} = \Delta G_{\text{Bound state}} - \Delta G_{\text{free state}}$. All units are in kcal/mol.

[c] Statistical uncertainties calculated for bidirectional (i.e., forward and backward transformation) FEP calculations using the BAR estimator are all between ± 0.03 to ± 0.18 kcal/mol.

Table 2.

Omicron BA.1 SARS-CoV-2 replicon with the S144A/E166A 3CLpro mutation has decreased susceptibility to nirmatrelvir.

Susceptibility of SARS-CoV-2 replicons to nirmatrelvir was assessed by Nanoluc activity. EC_{50} mean and standard deviations (SD) are determined from using both technical (n = 2) and biological (n = 2) replicates.

Omicron BA.1 strain (3CLpro variant)	EC_{50} ± SD (μM) (Fold change from WT BA.1)
$WT_{Omicron\ BA.1}$	0.11 ± 0.02 **(1)**
$(S144A/E166A)_{Omicron\ BA.1}$	2.22 ± 0.41 **(20)**